UCRL-JC-120504
PREPRINT

Overview of Reaction Mechanisms for Calculating the High Energy Component of Fast-Nucleon Induced Gamma Spectra

Frank S. Dietrich

This paper was prepared for submittal to the
First Research Coordination Meeting on Measurement,
Calculation and Evaluation of Photon Production Data
Bologna, Italy
November 14-17, 1994

February 21, 1995

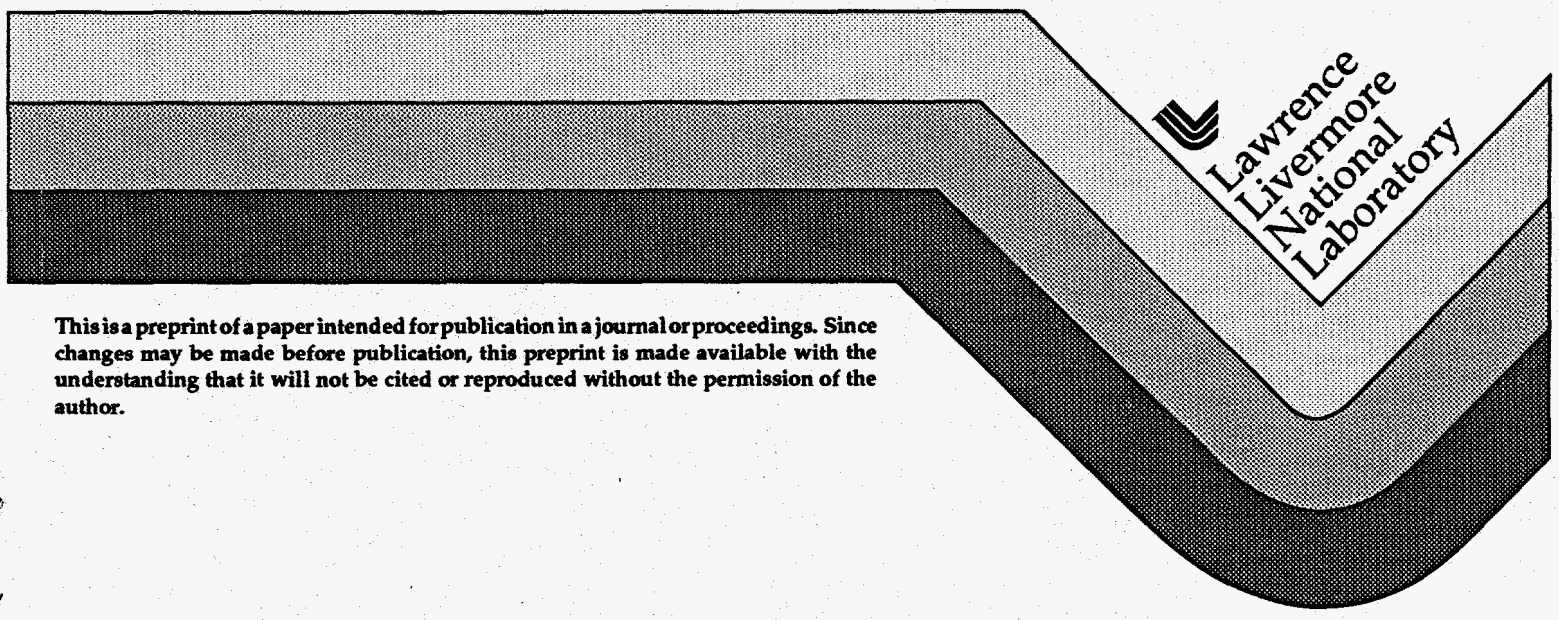

DISCLAIMER

OVERVIEW OF REACTION MECHANISMS FOR CALCULATING THE HIGH ENERGY COMPONENT OF FAST-NUCLEON INDUCED GAMMA SPECTRA

FRANK S. DIETRICH
Lawrence Livermore National Laboratory
P. O. Box 808, Livermore, CA 94550, USA

ABSTRACT

This presentation reviews the current status of quantum mechanical models for understanding the high-energy component of gamma spectra resulting from radiative capture of fast nucleons; i.e., the part of the spectrum that is not amenable to standard statistical model (Hauser-Feshbach) treatments. These models are based on the direct-semidirect (DSD) model and its variants. Included are recent results on the extension of the DSD model to unbound final states, a discussion of problems and improvements in understanding the form factors in this model, and a brief discussion of a model closely related to the DSD, the pure-resonance model.

1. Introduction

In radiative capture of nucleons above a few MeV incident energy, the most energetic gammas are well understood as arising from direct reaction processes. Since its introduction 30 years ago, the direct-semidirect (DSD) model[1,2] has been the principal theoretical tool for interpreting this component of the gamma spectrum. In this model, direct radiative capture is supplemented by additional coherent amplitudes in which the incident nucleon excites giant resonances that subsequently decay by gamma emission. While both types of amplitudes are required for a full description of the capture process, semidirect excitation of the giant-dipole resonance (GDR) is dominant over a wide energy region about the position of the GDR. In addition to the dominant E1 multipolarity, higher multipolarities (M1, E2, E3) have also been included in DSD calculations.

An important feature of the semidirect terms is the form factors that contain the physics of the coupling of the incident nucleon to the giant resonances. These form factors are derived from models for the transition densities of the giant resonances[3], and contain input from the strength of the isovector or isoscalar nucleon-nucleon interaction, as well as the fraction of an appropriate sum rule exhausted by the giant resonances; form factors for both isovector (E1, E2) and isoscalar (E2) resonances have been implemented. However, the details of the radial shape and strength of the form factors are poorly known. In particular, an imaginary component[4] in the form factor is required to achieve a phasing between the direct and semidirect terms that agrees with experiment, but its origin is not well understood. Section 3 below reviews an attempt to shed light on the real part of the form factor by employing a microscopic folding model which has proven successful

for calculating inelastic-scattering form factors as well as optical potentials. The importance of Coulomb excitation in calculating the form factors for proton capture is illustrated. New insights into the imaginary component of the form factors are contained in the contribution of A. Likar[5] to this meeting.

Up to the present, DSD calculations have been limited to capture to bound final states, and consequently only the portion of the gamma spectrum between the incident nucleon energy and the endpoint (approximately 8 MeV higher) has been available for this model. Consequently, the portion of the spectrum above the region where Hauser-Feshbach calculations apply (less than approximately 10-12 MeV) and below the region of bound final states has been calculated only with semiclassical pre-equilibrium models[6], or with multistep compound models that yield conflicting results[7,8]. A recent extension of the DSD model to unbound final states[9] that significantly expands the region of applicability of this model is reviewed in Section 2. This extended model is also applicable to a portion of the bound final-state region where conventional DSD calculations are of limited usefulness because of fragmentation of the final single-particle orbitals among a dense background of complicated neighboring states.

Difficulties in applying the DSD model to certain transitions in heavy nuclei (particularly neutron and proton capture on ^{208}Pb) led to the development of a closely related model, the pure-resonance model (PRM). This model[10,11], which is an approximation to DSD, was developed in the course of an examination of the consistency of the DSD model. A current view of this model and recent results using it are presented in Section 4.

2. The Extended DSD Model for Capture to Unstable Final States

The direct-semidirect model has recently been extended to allow calculation of radiative capture to unstable final states. Two types of unstable final states are included: 1) states in which the single-particle configuration following capture are unbound and may therefore decay into the continuum, and 2) single-particle states that are bound, but subsequently damp into the compound nucleus. In both cases, the correct treatment of the compound-nuclear damping is critical for the success of the model. The model has been tested by performing an experiment on radiative capture of 19.6-MeV polarized protons on ^{89}Y, and is described in a paper recently submitted for publication[9].

The principal difference between the extended treatment and the standard DSD model is in the handling of the final state. In the standard DSD model, the final state of the captured particle is described by a bound-state wave function, usually obtained by solution of the Schrödinger equation for a Woods-Saxon well. In the extension of the model, all necessary information on the final state is determined by a complex (i.e., optical) potential, which is defined for both unbound and bound final-state single-particle configurations. For unbound final states, the imaginary potential describes damping of the simple single-particle state following capture into the compound nucleus. Similarly, for bound final states, the imaginary potential represents the spreading of the single-particle configuration into a dense spectrum of complicated states in the neighborhood of the final-state energy.

The extended model reduces to the standard DSD calculation in the limit of vanishing final-state imaginary potential.

In the extended model for capture to unbound final-state configurations, the double-differential inclusive cross section (i.e., in which only the outgoing gamma is measured) is

$$\frac{d\sigma}{dE_\gamma d\Omega_\gamma} = \sigma_1 + \sigma_2 \ , \tag{1}$$

in which the first term on the right-hand side is

$$\sigma_1 = -\frac{1}{\phi_{inc}}\frac{2}{\hbar}\left(\frac{1}{\hbar c}\right)^3 E_\gamma^2 \ \left\langle \overline{\Psi}_i^{(+)} \middle| H_\gamma G^{(+)\dagger} W G^{(+)} H_\gamma \middle| \overline{\Psi}_i^{(+)} \right\rangle, \tag{2}$$

and the second is

$$\sigma_2 = \frac{1}{\phi_{inc}}\frac{2\pi}{\hbar}\left(\frac{1}{\hbar c}\right)^3 E_\gamma^2 \sum_{\mathbf{p}} \left| \left\langle \tilde{\chi}_{\mathbf{p}}^{(-)} \middle| H_\gamma \middle| \overline{\Psi}_i^{(+)} \right\rangle \right|^2 \delta(E - E_p). \tag{3}$$

For bound final-state configurations, the corresponding expression is

$$\frac{d\sigma}{dE_\gamma d\Omega_\gamma} = -\frac{1}{\phi_{inc}}\frac{2}{\hbar}\left(\frac{1}{\hbar c}\right)^3 E_\gamma^2 \ \mathrm{Im}\left\langle \overline{\Psi}_i^{(+)} \middle| H_\gamma G^{(+)} H_\gamma \middle| \overline{\Psi}_i^{(+)} \right\rangle . \tag{4}$$

In these expressions, $\overline{\Psi}_i^{(+)}$ is the energy-averaged incident wave function at energy E_i; it is the optical-model wave function, plus resonant terms representing coupling to giant resonances that give rise to the semidirect amplitude. E_f and E_γ are the energies of the final nuclear state and gamma ray, respectively, while E is $E_i - E_\gamma$. H_γ is the electromagnetic operator. ϕ_{inc} is the flux of incident particles. $G^{(+)}$ is a Green's function (with appropriate boundary conditions) for the interaction of the captured nucleon with the target via a complex optical potential. W is the imaginary part of the optical potential, defined for both continuum and bound final states, and $\tilde{\chi}_{\mathbf{p}}^{(-)}$ is an optical-model wave function for continuum final states. For the unbound case, Eq. (3) is the straightforward extension of the conventional DSD calculation. The additional term, Eq. (2), represents damping of the final-state configuration following capture, and in fact is the dominant term[9].

Calculations using the extended DSD model are shown in Figs. 1 and 2 and are compared to the results of the ^{89}Y(p,γ) experiment with 19.6-MeV polarized protons. Direct E1, E2, and E3 radiation as well as semidirect E1 were included.

Fig. 1 shows the measured 90° differential cross section, together with the extended DSD calculations and with Hauser-Feshbach calculations using the GNASH code[12] of the equilibrium statistical emission using two different prescriptions for the gamma-ray transmission coefficient[13,14]. The peak at 15.11 MeV is due to inelastic scattering on a carbon impurity in the target. The combination of DSD and Hauser-Feshbach calculations reproduces the data reasonably well, and additional multistep reaction mechanisms are not required. The DSD calculation were made with Eqs. (2) and (3) in the unbound region below 19.6 MeV gamma energy, and with Eq. (4) in the bound-state region above that energy. There is no discontinuity between these two regions. The DSD calculations were

carried out to only 26 MeV, since the ground-state peak near 28 MeV is more appropriately treated by a conventional DSD calculation. The calculations show a transition between compound and direct processes in the region near 16 MeV.

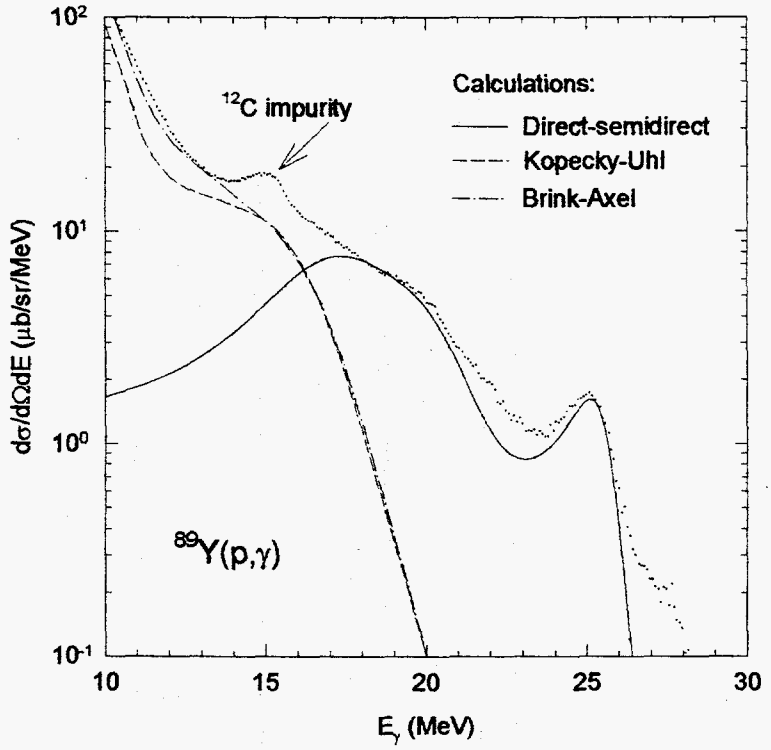

Figure 1. Unpolarized differential cross section at 90°. The data (dots) are shown together with the extended DSD model calculation (solid line), and with Hauser-Feshbach calculations using Kopecky-Uhl (dashed line) and Brink-Axel (dot-dashed line) gamma transmission coefficients. The calculations were folded with experimentally determined lineshapes before presentation with the data.

In Fig. 2 the extended DSD calculations are compared with the measured analyzing powers at the five angles for which data were taken. The data are well reproduced by the calculations, including the reversal in the sign of the asymmetries between the forward and backward hemispheres.

The calculations shown here suggest that multistep contributions may not be important at energies up to approximately 20 MeV. To further investigate this issue, the model is currently being applied to a set of gamma-production data taken with 34 MeV protons[15]. If the higher-energy data show that multistep contributions are required, the extended model will be incorporated as the final step in a multistep-direct theory based on the FKK reaction theory[16].

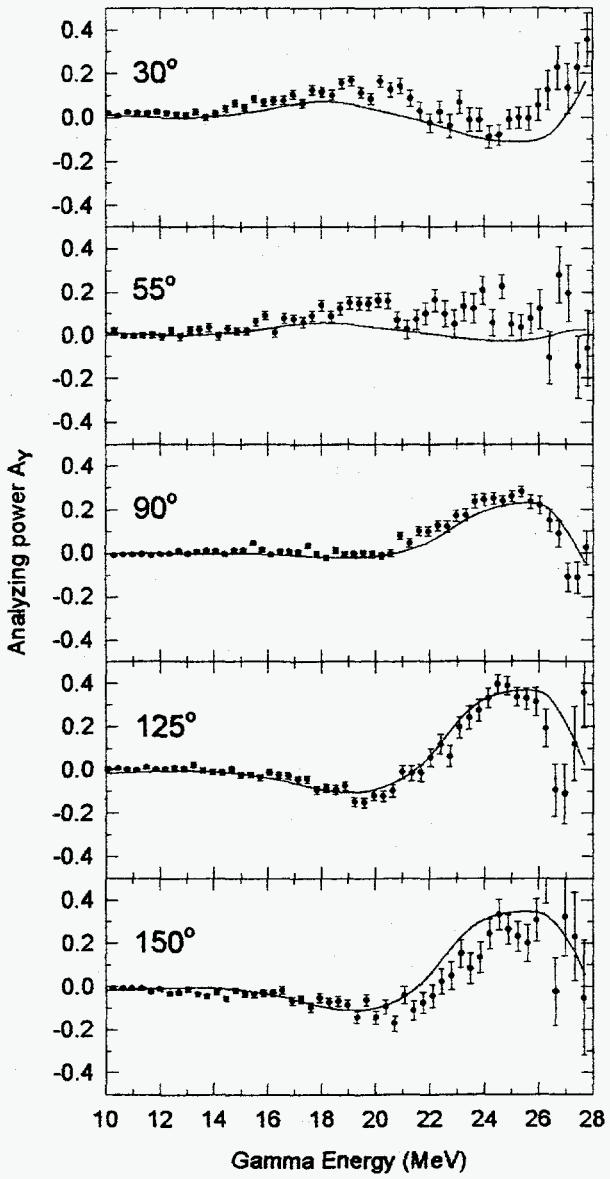

Figure 2. Measured analyzing powers compared with the extended DSD calculations. The calculations have been folded with the experimentally-determined lineshapes.

3. The Form Factor Used in Direct-Semidirect Calculations

As noted in the introduction, a correct description of the complex form factors for coupling to the giant resonances remains an important outstanding problem in the DSD model. There is an issue of consistency in the DSD model (noted below in Section 4) that may be best addressed through an improved treatment of the form factors. The form factors are similar to those used in the DBWA description of nucleon inelastic scattering. However, radiative capture in the DSD picture contains an ingredient that is not present in inelastic scattering: the direct-capture amplitude interferes with the semidirect amplitude, and this places additional demands on the form factor to assure the correct phasing. The imaginary component of the form factor, introduced phenomenologically[4], has been adjusted to fit experiments, but its origin is not well understood. A new approach to the imaginary form factor has been introduced elsewhere at this meeting[5]. There is also a great deal of variation in the prescriptions used for the real part of the form factor. Most treatments of the real part are based on hydrodynamic models; however, a microscopic approach based on a particle-hole description of the giant resonances is also possible.

This section reviews an early attempt[11] to calculate the real part of the form factor using a simple microscopic model for the giant dipole resonance. The shape of this form factor is significantly different from those obtained from hydrodynamic models. The results are similar to those presented in another microscopic treatment by Shubin at this meeting[17]. The contribution of Coulomb excitation to the form factor is easily calculated in a microscopic model, and the importance of this effect for proton capture is shown below.

The microscopic description of the form factor requires a description of the transition density for the giant resonance, which is convoluted with an effective interaction. In the calculation shown in Fig. 3, the transition density for the giant dipole resonance in ^{208}Pb was obtained from the random phase approximation (RPA) form of the Brown-Bolsterli schematic model, and is shown in the lower part of the figure. The effective interaction used to obtain the form factors shown in the upper part of the figure was taken from the isovector part of the microscopic optical potential of Jeukenne, Lejeune, and Mahaux[18] (JLM). This interaction is complex, and is energy and density dependent. Only the real part of the interaction was used, since the strong energy dependence of the imaginary part leads to an ambiguity in the calculation of the imaginary form factor (i.e., the energy at which the interaction should be evaluated for capture from the continuum to a bound state is ill defined). The strength of the JLM isovector interaction has been normalized upward by a factor of 2.5, which is in accord with the normalization required to reproduce the (p,n) reaction to isobaric analog states[19]. For proton capture, the Coulomb excitation contribution was calculated by convoluting the transition density with an electromagnetic interaction of the form $1/r^2$.

The resulting form factors for proton and neutron capture shown in Fig. 3 peak at significantly larger radii than those for hydrodynamic models. The curve labeled B-G is a typical volume-type hydrodynamic form factor using the isovector strength and geometry

of the Becchetti-Greenlees[20] optical potential. The approximately 25% difference between the proton and neutron microscopic calculations is due almost entirely to the effect of Coulomb excitation. Coulomb excitation thus contributes significantly to the proton form factor, since the capture cross section near the peak of the giant resonance is nearly proportional to the square of the strength of the form factor. It should be noted that the microscopic form factor peaks at a larger radius than the transition density; this is a consequence of the density dependence of the effective interaction. It would be desirable to carry out a systematic comparison of DSD calculations with data using a microscopic form factor for the real part of the GDR coupling, supplemented by a phenomenological form for the imaginary part.

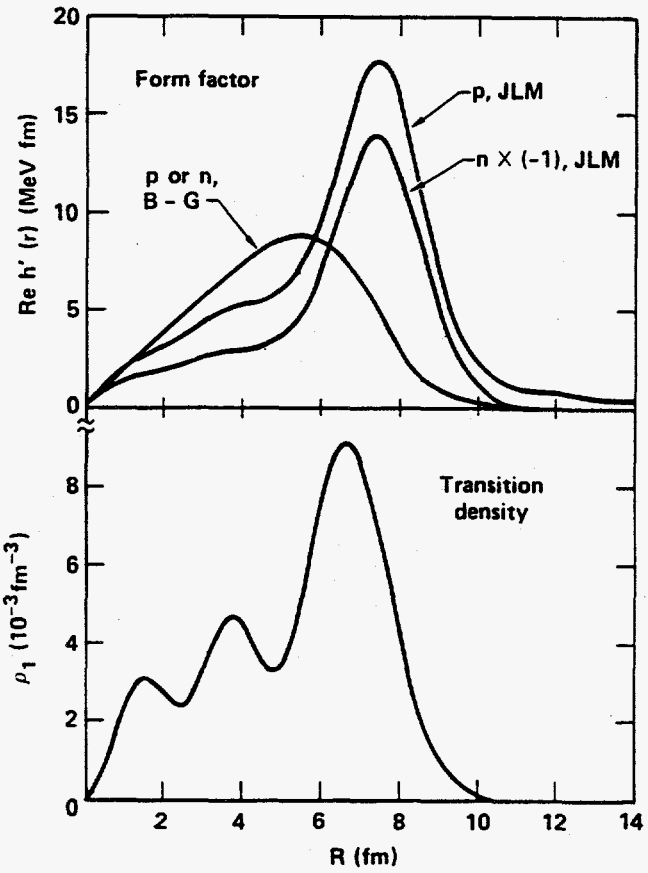

Figure 3. Folding-model calculation of the real part of the GDR form factor for ^{208}Pb, based on a schematic-model description of the transition density and the JLM effective interaction. The curve labeled B-G is a hydronamic form factor shown for comparison. The difference between proton and neutron microscopic form factors is due to Coulomb excitation.

4. The Pure-Resonance Model

The pure-resonance model[10,11] (PRM) was developed to address questions of consistency between the two terms in the direct-semidirect model. It was based on the two observations that 1) in the photoejection reaction (which is inverse to radiative capture) experimental data show symmetric resonant peaks without an obvious nonresonant contribution; and that 2) the direct amplitude in DSD contains a giant-resonance contribution, since the incident optical-model wave function is not orthogonal to the giant resonance.

The PRM results from reformulating the capture model so that the continuum wave function appearing in its matrix elements no longer contains giant-resonance components. This is accomplished by using projection operator techniques as developed for the photonuclear problem by Wang and Shakin[21]. Using these techniques, the direct-semidirect amplitude

$$c_1 + \frac{c_2}{E_\gamma - E_{GDR} + \frac{1}{2} i\Gamma_{GDR}} \tag{5}$$

may be formally rearranged (neglecting an unimportant small term) as

$$\frac{c_3 - c_4}{E_\gamma - E_{SP} + \frac{1}{2} i\Gamma_{SP}} + \frac{c_5}{E_\gamma - E_{GDR} + \frac{1}{2} i\Gamma_{GDR}} \tag{6}$$

in which c_1 through c_5 are matrix elements calculated with ordinary optical wave functions in the DSD case (Eq. (5)), or projected wave functions for the PRM (Eq. (6)). E_{SP} and Γ_{SP} are the position and width of a single-particle resonance in the entrance channel, and are computed from the optical potential. The single particle resonance lies in the region of approximately 8 to 10 MeV. E_{GDR} and Γ_{GDR} are the position and width of the giant dipole resonance.

In Eq. (6), c_3 and c_4 are both large and nearly cancel. Thus, a potential instability that is implicit in the DSD model is exhibited explicitly in the PRM formulation. In the pure-resonance model this instability is eliminated by assuming that this cancellation is exact, leaving only the giant resonance term.

A recent experiment[22] on the $^{40}Ca(n,\gamma_0)$ reaction, which was performed to search for the isovector quadrupole giant resonance, shows the usefulness of the PRM. Fig. 4 shows the data for this reaction, together with two calculations that included E1 and E2 radiation. The right-hand panel shows the 90° differential cross section, while the left-hand shows the fore-aft asymmetry A(55°), defined as $[\sigma(55°)- \sigma(125°)]/[\sigma(55°)+\sigma(125°)]$, where σ is the differential cross section. The solid curves used DSD for both E1 and E2, whereas the dashed curves were calculated using PRM for E1 and DSD for E2.

In the case shown in Fig. 4, it is apparent that the PRM yields a better reproduction of the experiment than the DSD. However, it should be noted that the approximation of neglecting the first term in Eq. (6) may be extreme, and that this approximation may not be necessary if the consistency between the direct and semidirect terms in the DSD model is better understood than at present. Further work should be done in this direction.

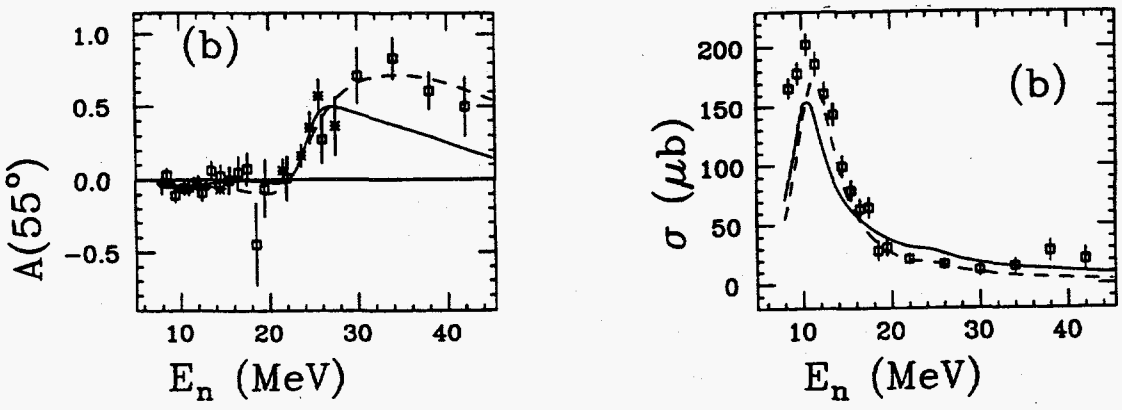

Figure 4. Fore-aft asymmetry (left panel) and 90° differential cross section (right panel) in the $^{40}Ca(n,\gamma_0)$ reaction[22]. Calculations were made with DSD for E1 and E2 amplitudes (solid curves), and with PRM for E1 and DSD for E2 (dashed curves).

5. Acknowledgment

The work required for the preparation of this review was supported by the Lawrence Livermore National Laboratory under United States Department of Energy contract W-7405-ENG-48.

6. References

1. G. E. Brown, Nucl. Phys. **57**, 339 (1964).
2. C. F. Clement, A. M. Lane, and J. R. Rook, Nucl. Phys. **66**, 273,293 (1965).
3. G. R. Satchler, Nucl. Phys. **A195**, 1 (1972).
4. M. Potokar, Phys. Lett. **46B**, 346 (1973).
5. A. Likar, contribution to this meeting.
6. E. Betak, contribution to this meeting and references therein.
7. P. Oblozinsky and M. Chadwick, Phys. Rev. **C42**, 1652 (1990).
8. M. Herman, A. Höring, and G. Reffo, Phys. Rev. **C46**, 2493 (1992).
9. W. E. Parker *et al.*, submitted to Physical Review **C**.
10. F. S. Dietrich and A. K. Kerman, Phys. Rev. Lett. **43**, 114 (1979).
11. F. S. Dietrich, in AIP Conference Proceedings No. 125, Capture Gamma-Ray Spectroscopy, Knoxville, TN, 1984, p. 445.
12. P. G. Young, E. D. Arthur, and M. B. Chadwick, Los Alamos National Laboratory Report LA-12343-MS (1992).

13. D. M. Brink, Ph. D. thesis, Oxford University (1955); P. Axel, Phys. Rev. **126**, 671 (1962).
14. J. Kopecky and M. Uhl, Phys. Rev. **C41**, 1941 (1990).
15. S. J. Luke, Ph.D. thesis, University of Washington, 1992.
16. H. Feshbach, A. K. Kerman, and S. Koonin, Ann. Phys. (New York) **125**, 429 (1980).
17. Yu. Shubin, contribution to this meeting.
18. J. P. Jeukenne, A. Lejeune, and C. Mahaux, Phys. Rev. **C16**, 80 (1977), and references therein.
19. F. S. Dietrich and F. Petrovich, in AIP Conference Proceedings No. 124, Neutron-Nucleus Collisions -- A Probe of Nuclear Structure, Burr Oak State Park, Ohio, 1984, p. 90.
20. F. D. Becchetti and G. W. Greenlees, Phys. Rev. **182**, 1190 (1969).
21. W. L. Wang and C. M. Shakin, Phys. Rev. **C5**, 1898 (1972).
22. C. M. Laymon, R. O. Nelson, S. A. Wender, and L. R. Nilsson, Phys. Rev. **C46**, 1880 (1992).